

# Measurements at forward rapidity of elliptic flow of charged hadrons and open-heavy-flavor muons in Au+Au collisions at $\sqrt{s_{NN}} = 200$ GeV

N.J. Abdulameer,<sup>15,22</sup> U. Acharya,<sup>19</sup> A. Adare,<sup>12</sup> C. Aidala,<sup>42</sup> N.N. Ajitanand,<sup>61,\*</sup> Y. Akiba,<sup>56,57,†</sup> M. Alfred,<sup>21</sup> S. Antsupov,<sup>59</sup> K. Aoki,<sup>31,56</sup> N. Apadula,<sup>27,62</sup> H. Asano,<sup>34,56</sup> C. Ayuso,<sup>42</sup> B. Azmoun,<sup>7</sup> V. Babintsev,<sup>23</sup> M. Bai,<sup>6</sup> N.S. Bandara,<sup>40</sup> B. Bannier,<sup>62</sup> E. Bannikov,<sup>59</sup> K.N. Barish,<sup>8</sup> S. Bathe,<sup>5,57</sup> A. Bazilevsky,<sup>7</sup> M. Beaumier,<sup>8</sup> S. Beckman,<sup>12</sup> R. Belmont,<sup>12,49</sup> A. Berdnikov,<sup>59</sup> Y. Berdnikov,<sup>59</sup> L. Bichon,<sup>67</sup> B. Blankenship,<sup>67</sup> D.S. Blau,<sup>33,46</sup> M. Boer,<sup>36</sup> J.S. Bok,<sup>48</sup> V. Borisov,<sup>59</sup> K. Boyle,<sup>57</sup> M.L. Brooks,<sup>36</sup> J. Bryslawskyj,<sup>5,8</sup> V. Bumazhnov,<sup>23</sup> C. Butler,<sup>19</sup> S. Campbell,<sup>13,27</sup> V. Canoa Roman,<sup>62</sup> C.-H. Chen,<sup>57</sup> D. Chen,<sup>62</sup> M. Chiu,<sup>7</sup> C.Y. Chi,<sup>13</sup> I.J. Choi,<sup>24</sup> J.B. Choi,<sup>29,\*</sup> T. Chujo,<sup>65</sup> Z. Citron,<sup>68</sup> M. Connors,<sup>19,57</sup> R. Corliss,<sup>62</sup> M. Csanád,<sup>16</sup> T. Csörgő,<sup>41,69</sup> L. D. Liu,<sup>53</sup> T.W. Danley,<sup>50</sup> A. Datta,<sup>47</sup> M.S. Daugherty,<sup>1</sup> G. David,<sup>7,62</sup> K. DeBlasio,<sup>47</sup> K. Dehmelt,<sup>62</sup> A. Denisov,<sup>23</sup> A. Deshpande,<sup>57,62</sup> E.J. Desmond,<sup>7</sup> A. Dion,<sup>62</sup> P.B. Diss,<sup>39</sup> V. Doomra,<sup>62</sup> J.H. Do,<sup>70</sup> A. Drees,<sup>62</sup> K.A. Drees,<sup>6</sup> M. Dumancic,<sup>68</sup> J.M. Durham,<sup>36</sup> A. Durum,<sup>23</sup> T. Elder,<sup>19</sup> A. Enokizono,<sup>56,58</sup> R. Esha,<sup>62</sup> B. Fadem,<sup>44</sup> W. Fan,<sup>62</sup> N. Feege,<sup>62</sup> D.E. Fields,<sup>47</sup> M. Finger, Jr.,<sup>9</sup> M. Finger,<sup>9</sup> D. Firak,<sup>15,62</sup> D. Fitzgerald,<sup>42</sup> S.L. Fokin,<sup>33</sup> J.E. Frantz,<sup>50</sup> A. Franz,<sup>7</sup> A.D. Frawley,<sup>18</sup> Y. Fukuda,<sup>65</sup> P. Gallus,<sup>14</sup> C. Gal,<sup>62</sup> P. Garg,<sup>3,62</sup> H. Ge,<sup>62</sup> F. Giordano,<sup>24</sup> A. Glenn,<sup>35</sup> Y. Goto,<sup>56,57</sup> N. Grau,<sup>2</sup> S.V. Greene,<sup>67</sup> M. Grosse Perdekamp,<sup>24</sup> T. Gunji,<sup>11</sup> T. Guo,<sup>62</sup> T. Hachiya,<sup>56,57</sup> J.S. Haggerty,<sup>7</sup> K.I. Hahn,<sup>17</sup> H. Hamagaki,<sup>11</sup> H.F. Hamilton,<sup>1</sup> J. Hanks,<sup>62</sup> S.Y. Han,<sup>17,32</sup> S. Hasegawa,<sup>28</sup> T.O.S. Haseler,<sup>19</sup> K. Hashimoto,<sup>56,58</sup> T.K. Hemmick,<sup>62</sup> X. He,<sup>19</sup> J.C. Hill,<sup>27</sup> K. Hill,<sup>12</sup> A. Hodges,<sup>19,24</sup> R.S. Hollis,<sup>8</sup> K. Homma,<sup>20</sup> B. Hong,<sup>32</sup> T. Hoshino,<sup>20</sup> N. Hotvedt,<sup>27</sup> J. Huang,<sup>7</sup> K. Imai,<sup>28</sup> J. Imrek,<sup>15</sup> M. Inaba,<sup>65</sup> A. Iordanova,<sup>8</sup> D. Isenhower,<sup>1</sup> Y. Ito,<sup>45</sup> D. Ivanishchev,<sup>55</sup> B. Jacak,<sup>62</sup> M. Jezghani,<sup>19</sup> X. Jiang,<sup>36</sup> Z. Ji,<sup>62</sup> B.M. Johnson,<sup>7,19</sup> V. Jorjadze,<sup>62</sup> D. Jouan,<sup>52</sup> D.S. Jumper,<sup>24</sup> S. Kanda,<sup>11</sup> J.H. Kang,<sup>70</sup> D. Kapukchyan,<sup>8</sup> S. Karthas,<sup>62</sup> D. Kawall,<sup>40</sup> A.V. Kazantsev,<sup>33</sup> J.A. Key,<sup>47</sup> V. Khachatryan,<sup>62</sup> A. Khazadzev,<sup>55</sup> B. Kimelman,<sup>44</sup> C. Kim,<sup>8,32</sup> D.J. Kim,<sup>30</sup> E.-J. Kim,<sup>29</sup> G.W. Kim,<sup>17</sup> M. Kim,<sup>60</sup> M.H. Kim,<sup>32</sup> D. Kincses,<sup>16</sup> E. Kistenev,<sup>7</sup> R. Kitamura,<sup>11</sup> J. Klatsky,<sup>18</sup> D. Kleinjan,<sup>8</sup> P. Kline,<sup>62</sup> T. Koblesky,<sup>12</sup> B. Komkov,<sup>55</sup> D. Kotov,<sup>55,59</sup> L. Kovacs,<sup>16</sup> S. Kudo,<sup>65</sup> K. Kurita,<sup>58</sup> M. Kurosawa,<sup>56,57</sup> Y. Kwon,<sup>70</sup> J.G. Lajoie,<sup>27,51</sup> E.O. Lallow,<sup>44</sup> A. Lebedev,<sup>27</sup> S. Lee,<sup>70</sup> S.H. Lee,<sup>27,62</sup> M.J. Leitch,<sup>36</sup> Y.H. Leung,<sup>62</sup> N.A. Lewis,<sup>42</sup> S.H. Lim,<sup>36,54,70</sup> M.X. Liu,<sup>36</sup> X. Li,<sup>10</sup> X. Li,<sup>36</sup> V.-R. Loggins,<sup>24</sup> S. Lökös,<sup>69</sup> D.A. Loomis,<sup>42</sup> D. Lynch,<sup>7</sup> T. Majoros,<sup>15</sup> Y.I. Makdisi,<sup>6</sup> M. Makek,<sup>71</sup> M. Malaev,<sup>55</sup> A. Manion,<sup>62</sup> V.I. Manko,<sup>33</sup> E. Mannel,<sup>7</sup> H. Masuda,<sup>58</sup> M. McCumber,<sup>36</sup> P.L. McGaughey,<sup>36</sup> D. McGlinchey,<sup>12,36</sup> C. McKinney,<sup>24</sup> A. Meles,<sup>48</sup> M. Mendoza,<sup>8</sup> A.C. Mignerey,<sup>39</sup> D.E. Mihalik,<sup>62</sup> A. Milov,<sup>68</sup> D.K. Mishra,<sup>4</sup> J.T. Mitchell,<sup>7</sup> M. Mitrankova,<sup>59,62</sup> Iu. Mitrankov,<sup>59,62</sup> G. Mitsuka,<sup>31,57</sup> S. Miyasaka,<sup>56,64</sup> S. Mizuno,<sup>56,65</sup> A.K. Mohanty,<sup>4</sup> P. Montuenga,<sup>24</sup> T. Moon,<sup>32,70</sup> D.P. Morrison,<sup>7</sup> S.I. Morrow,<sup>67</sup> T.V. Moukhanova,<sup>33</sup> B. Mulilo,<sup>32,56,72</sup> T. Murakami,<sup>34,56</sup> J. Murata,<sup>56,58</sup> A. Mwai,<sup>61</sup> K. Nagai,<sup>64</sup> K. Nagashima,<sup>20</sup> T. Nagashima,<sup>58</sup> J.L. Nagle,<sup>12</sup> M.I. Nagy,<sup>16</sup> I. Nakagawa,<sup>56,57</sup> H. Nakagomi,<sup>56,65</sup> K. Nakano,<sup>56,64</sup> C. Nattrass,<sup>63</sup> P.K. Netrakanti,<sup>4</sup> T. Niida,<sup>65</sup> S. Nishimura,<sup>11</sup> R. Nouicer,<sup>7,57</sup> N. Novitzky,<sup>30,62</sup> R. Novotny,<sup>14</sup> T. Novák,<sup>41,69</sup> G. Nukazuka,<sup>56,57</sup> A.S. Nyanin,<sup>33</sup> E. O'Brien,<sup>7</sup> C.A. Ogilvie,<sup>27</sup> J.D. Orjuela Koop,<sup>12</sup> M. Orosz,<sup>15,22</sup> J.D. Osborn,<sup>42,51</sup> A. Oskarsson,<sup>37</sup> K. Ozawa,<sup>31,65</sup> R. Pak,<sup>7</sup> V. Pantuev,<sup>25</sup> V. Papavassiliou,<sup>48</sup> J.S. Park,<sup>60</sup> S. Park,<sup>43,56,60,62</sup> M. Patel,<sup>27</sup> S.F. Pate,<sup>48</sup> J.-C. Peng,<sup>24</sup> W. Peng,<sup>67</sup> D.V. Perepelitsa,<sup>7,12</sup> G.D.N. Perera,<sup>48</sup> D.Yu. Peressounko,<sup>33</sup> C.E. PerezLara,<sup>62</sup> J. Perry,<sup>27</sup> R. Petti,<sup>7,62</sup> M. Phipps,<sup>7,24</sup> C. Pinkenburg,<sup>7</sup> R. Pinson,<sup>1</sup> R.P. Pisani,<sup>7</sup> M. Potekhin,<sup>7</sup> A. Pun,<sup>50</sup> M.L. Purschke,<sup>7</sup> J. Rak,<sup>30</sup> B.J. Ramson,<sup>42</sup> I. Ravinovich,<sup>68</sup> K.F. Read,<sup>51,63</sup> D. Reynolds,<sup>61</sup> V. Riabov,<sup>46,55</sup> Y. Riabov,<sup>55,59</sup> D. Richford,<sup>5,66</sup> T. Rinn,<sup>27</sup> S.D. Rolnick,<sup>8</sup> M. Rosati,<sup>27</sup> Z. Rowan,<sup>5</sup> J.G. Rubin,<sup>42</sup> J. Runchey,<sup>27</sup> B. Sahlmueller,<sup>62</sup> N. Saito,<sup>31</sup> T. Sakaguchi,<sup>7</sup> H. Sako,<sup>28</sup> V. Samsonov,<sup>46,55</sup> M. Sarsour,<sup>19</sup> K. Sato,<sup>65</sup> S. Sato,<sup>28</sup> B. Schaefer,<sup>67</sup> B.K. Schmoll,<sup>63</sup> K. Sedgwick,<sup>8</sup> R. Seidl,<sup>56,57</sup> A. Seleznev,<sup>59</sup> A. Sen,<sup>27,63</sup> R. Seto,<sup>8</sup> P. Sett,<sup>4</sup> A. Sexton,<sup>39</sup> D. Sharma,<sup>62</sup> I. Shein,<sup>23</sup> T.-A. Shibata,<sup>56,64</sup> K. Shigaki,<sup>20</sup> M. Shimomura,<sup>27,45</sup> P. Shukla,<sup>4</sup> A. Sickles,<sup>7,24</sup> C.L. Silva,<sup>36</sup> D. Silvermyr,<sup>37,51</sup> B.K. Singh,<sup>3</sup> C.P. Singh,<sup>3,\*</sup> V. Singh,<sup>3</sup> M. Slunečka,<sup>9</sup> K.L. Smith,<sup>18,36</sup> M. Snowball,<sup>36</sup> R.A. Soltz,<sup>35</sup> W.E. Sondheim,<sup>36</sup> S.P. Sorensen,<sup>63</sup> I.V. Sourikova,<sup>7</sup> P.W. Stankus,<sup>51</sup> M. Stepanov,<sup>40,\*</sup> S.P. Stoll,<sup>7</sup> T. Sugitate,<sup>20</sup> A. Sukhanov,<sup>7</sup> T. Sumita,<sup>56</sup> J. Sun,<sup>62</sup> Z. Sun,<sup>15,22,62</sup> S. Syed,<sup>19</sup> J. Sziklai,<sup>69</sup> A. Takeda,<sup>45</sup> A. Taketani,<sup>56,57</sup> K. Tanida,<sup>28,57,60</sup> M.J. Tannenbaum,<sup>7</sup> S. Tarafdar,<sup>67,68</sup> A. Taranenko,<sup>46,61</sup> G. Tarnai,<sup>15</sup> R. Tieulent,<sup>19,38</sup> A. Timilsina,<sup>27</sup> T. Todoroki,<sup>56,57,65</sup> M. Tomášek,<sup>14</sup> C.L. Towell,<sup>1</sup> R. Towell,<sup>1</sup> R.S. Towell,<sup>1</sup> I. Tserruya,<sup>68</sup> Y. Ueda,<sup>20</sup> B. Ujvari,<sup>15,22</sup> H.W. van Hecke,<sup>36</sup> S. Vazquez-Carson,<sup>12</sup> J. Velkovska,<sup>67</sup> M. Virius,<sup>14</sup> V. Vrba,<sup>14,26</sup> X.R. Wang,<sup>48,57</sup> Z. Wang,<sup>5</sup> Y. Watanabe,<sup>56,57</sup> Y.S. Watanabe,<sup>11,31</sup> F. Wei,<sup>48</sup> A.S. White,<sup>42</sup> C.P. Wong,<sup>7,19,36</sup> C.L. Woody,<sup>7</sup> M. Wysocki,<sup>51</sup> B. Xia,<sup>50</sup> L. Xue,<sup>19</sup> C. Xu,<sup>48</sup> Q. Xu,<sup>67</sup> S. Yalcin,<sup>62</sup> Y.L. Yamaguchi,<sup>11,57,62</sup> A. Yanovich,<sup>23</sup> P. Yin,<sup>12</sup> I. Yoon,<sup>60</sup> J.H. Yoo,<sup>32</sup> I.E. Yushmanov,<sup>33</sup> H. Yu,<sup>48,53</sup> W.A. Zajc,<sup>13</sup> A. Zelenski,<sup>6</sup> S. Zhou,<sup>10</sup> and L. Zou<sup>8</sup>

(PHENIX Collaboration)

- <sup>1</sup> Abilene Christian University, Abilene, Texas 79699, USA
- <sup>2</sup> Department of Physics, Augustana University, Sioux Falls, South Dakota 57197, USA
- <sup>3</sup> Department of Physics, Banaras Hindu University, Varanasi 221005, India
- <sup>4</sup> Bhabha Atomic Research Centre, Bombay 400 085, India
- <sup>5</sup> Baruch College, City University of New York, New York, New York, 10010 USA
- <sup>6</sup> Collider-Accelerator Department, Brookhaven National Laboratory, Upton, New York 11973-5000, USA
- <sup>7</sup> Physics Department, Brookhaven National Laboratory, Upton, New York 11973-5000, USA
- <sup>8</sup> University of California-Riverside, Riverside, California 92521, USA
- <sup>9</sup> Charles University, Faculty of Mathematics and Physics, 180 00 Troja, Prague, Czech Republic
- <sup>10</sup> Science and Technology on Nuclear Data Laboratory, China Institute of Atomic Energy, Beijing 102413, People's Republic of China
- <sup>11</sup> Center for Nuclear Study, Graduate School of Science, University of Tokyo, 7-3-1 Hongo, Bunkyo, Tokyo 113-0033, Japan
- <sup>12</sup> University of Colorado, Boulder, Colorado 80309, USA
- <sup>13</sup> Columbia University, New York, New York 10027 and Nevis Laboratories, Irvington, New York 10533, USA
- <sup>14</sup> Czech Technical University, Zikova 4, 166 36 Prague 6, Czech Republic
- <sup>15</sup> Debrecen University, H-4010 Debrecen, Egyetem tér 1, Hungary
- <sup>16</sup> ELTE, Eötvös Loránd University, H-1117 Budapest, Pázmány P. s. 1/A, Hungary
- <sup>17</sup> Ewha Womans University, Seoul 120-750, Korea
- <sup>18</sup> Florida State University, Tallahassee, Florida 32306, USA
- <sup>19</sup> Georgia State University, Atlanta, Georgia 30303, USA
- <sup>20</sup> Physics Program and International Institute for Sustainability with Knotted Chiral Meta Matter (SKCM2), Hiroshima University, Higashi-Hiroshima, Hiroshima 739-8526, Japan
- <sup>21</sup> Department of Physics and Astronomy, Howard University, Washington, DC 20059, USA
- <sup>22</sup> HUN-REN ATOMKI, H-4026 Debrecen, Bem tér 18/c, Hungary
- <sup>23</sup> IHEP Protvino, State Research Center of Russian Federation, Institute for High Energy Physics, Protvino, 142281, Russia
- <sup>24</sup> University of Illinois at Urbana-Champaign, Urbana, Illinois 61801, USA
- <sup>25</sup> Institute for Nuclear Research of the Russian Academy of Sciences, prospekt 60-letiya Oktyabrya 7a, Moscow 117312, Russia
- <sup>26</sup> Institute of Physics, Academy of Sciences of the Czech Republic, Na Slovance 2, 182 21 Prague 8, Czech Republic
- <sup>27</sup> Iowa State University, Ames, Iowa 50011, USA
- <sup>28</sup> Advanced Science Research Center, Japan Atomic Energy Agency, 2-4 Shirakata Shirane, Tokai-mura, Naka-gun, Ibaraki-ken 319-1195, Japan
- <sup>29</sup> Jeonbuk National University, Jeonju, 54896, Korea
- <sup>30</sup> Helsinki Institute of Physics and University of Jyväskylä, P.O.Box 35, FI-40014 Jyväskylä, Finland
- <sup>31</sup> KEK, High Energy Accelerator Research Organization, Tsukuba, Ibaraki 305-0801, Japan
- <sup>32</sup> Korea University, Seoul 02841, Korea
- <sup>33</sup> National Research Center "Kurchatov Institute", Moscow, 123098 Russia
- <sup>34</sup> Kyoto University, Kyoto 606-8502, Japan
- <sup>35</sup> Lawrence Livermore National Laboratory, Livermore, California 94550, USA
- <sup>36</sup> Los Alamos National Laboratory, Los Alamos, New Mexico 87545, USA
- <sup>37</sup> Department of Physics, Lund University, Box 118, SE-221 00 Lund, Sweden
- <sup>38</sup> IPNL, CNRS/IN2P3, Univ Lyon, Université Lyon 1, F-69622, Villeurbanne, France
- <sup>39</sup> University of Maryland, College Park, Maryland 20742, USA
- <sup>40</sup> Department of Physics, University of Massachusetts, Amherst, Massachusetts 01003-9337, USA
- <sup>41</sup> MATE, Laboratory of Femtoscopy, Károly Róbert Campus, H-3200 Gyöngyös, Mátrai út 36, Hungary
- <sup>42</sup> Department of Physics, University of Michigan, Ann Arbor, Michigan 48109-1040, USA
- <sup>43</sup> Mississippi State University, Mississippi State, Mississippi 39762, USA
- <sup>44</sup> Muhlenberg College, Allentown, Pennsylvania 18104-5586, USA
- <sup>45</sup> Nara Women's University, Kita-uoya Nishi-machi Nara 630-8506, Japan
- <sup>46</sup> National Research Nuclear University, MEPhI, Moscow Engineering Physics Institute, Moscow, 115409, Russia
- <sup>47</sup> University of New Mexico, Albuquerque, New Mexico 87131, USA
- <sup>48</sup> New Mexico State University, Las Cruces, New Mexico 88003, USA
- <sup>49</sup> Physics and Astronomy Department, University of North Carolina at Greensboro, Greensboro, North Carolina 27412, USA
- <sup>50</sup> Department of Physics and Astronomy, Ohio University, Athens, Ohio 45701, USA
- <sup>51</sup> Oak Ridge National Laboratory, Oak Ridge, Tennessee 37831, USA
- <sup>52</sup> IPN-Orsay, Univ. Paris-Sud, CNRS/IN2P3, Université Paris-Saclay, BP1, F-91406, Orsay, France
- <sup>53</sup> Peking University, Beijing 100871, People's Republic of China
- <sup>54</sup> Pusan National University, Pusan 46241, Korea
- <sup>55</sup> PNPI, Petersburg Nuclear Physics Institute, Gatchina, Leningrad region, 188300, Russia
- <sup>56</sup> RIKEN Nishina Center for Accelerator-Based Science, Wako, Saitama 351-0198, Japan
- <sup>57</sup> RIKEN BNL Research Center, Brookhaven National Laboratory, Upton, New York 11973-5000, USA
- <sup>58</sup> Physics Department, Rikkyo University, 3-34-1 Nishi-Ikebukuro, Toshima, Tokyo 171-8501, Japan
- <sup>59</sup> Saint Petersburg State Polytechnic University, St. Petersburg, 195251 Russia
- <sup>60</sup> Department of Physics and Astronomy, Seoul National University, Seoul 151-742, Korea
- <sup>61</sup> Chemistry Department, Stony Brook University, SUNY, Stony Brook, New York 11794-3400, USA

<sup>62</sup>*Department of Physics and Astronomy, Stony Brook University, SUNY, Stony Brook, New York 11794-3800, USA*

<sup>63</sup>*University of Tennessee, Knoxville, Tennessee 37996, USA*

<sup>64</sup>*Department of Physics, Tokyo Institute of Technology, Oh-okayama, Meguro, Tokyo 152-8551, Japan*

<sup>65</sup>*Tomonaga Center for the History of the Universe, University of Tsukuba, Tsukuba, Ibaraki 305, Japan*

<sup>66</sup>*United States Merchant Marine Academy, Kings Point, New York 11024, USA*

<sup>67</sup>*Vanderbilt University, Nashville, Tennessee 37235, USA*

<sup>68</sup>*Weizmann Institute, Rehovot 76100, Israel*

<sup>69</sup>*Institute for Particle and Nuclear Physics, HUN-REN Wigner Research Centre for Physics, (HUN-REN Wigner RCP, RMI), H-1525 Budapest 114, POBox 49, Budapest, Hungary*

<sup>70</sup>*Yonsei University, IPAP, Seoul 120-749, Korea*

<sup>71</sup>*Department of Physics, Faculty of Science, University of Zagreb, Bijenička c. 32 HR-10002 Zagreb, Croatia*

<sup>72</sup>*Department of Physics, School of Natural Sciences, University of Zambia, Great East Road Campus, Box 32379, Lusaka, Zambia*

(Dated: September 20, 2024)

We present the first forward-rapidity measurements of elliptic anisotropy of open-heavy-flavor muons at the Relativistic Heavy Ion Collider. The measurements are based on data samples of Au+Au collisions at  $\sqrt{s_{NN}} = 200$  GeV collected by the PHENIX experiment in 2014 and 2016 with integrated luminosity of  $14.5 \text{ nb}^{-1}$ . The measurements are performed in the pseudorapidity range  $1.2 < |\eta| < 2$  and cover transverse momenta  $1 < p_T < 4$  GeV/c. The elliptic flow of charged hadrons as a function of transverse momentum is also measured in the same kinematic range. We observe significant elliptic flow for both charged hadrons and heavy-flavor muons. The results show clear mass ordering of elliptic flow of light- and heavy-flavor particles. The magnitude of the measured  $v_2$  is comparable to that in the midrapidity region. This indicates that there is no strong longitudinal dependence in the quark-gluon-plasma evolution between midrapidity and the rapidity range of this measurement at  $\sqrt{s_{NN}} = 200$  GeV.

## I. INTRODUCTION

The quark-gluon plasma (QGP) formed in high-energy heavy ion collisions [1–4] is a hot, dense state of matter comprised of strongly interacting quarks and gluons. A key property of QGP is its near-perfect-fluid behavior characterized by the azimuthal anisotropy of the produced particles, which is correlated with anisotropies in the initial-state energy density [5]. The elliptic azimuthal anisotropy ( $v_2$ ) is defined by the amplitude of the second harmonic in a Fourier series expansion of the azimuthal distribution of produced particles,

$$\frac{dN}{d\phi} \propto 1 + \sum_n 2v_n \cos[n(\phi - \Psi_n)] \quad (1)$$

where  $v_n = \langle \cos[n(\phi - \Psi_n)] \rangle$  is the  $n^{\text{th}}$  order flow coefficient,  $\phi$  is the azimuthal angle of any given particle, and  $\Psi_n$  is the angle of the  $n^{\text{th}}$ -order symmetry plane.

Theoretical approaches involve quantum chromodynamics (QCD). Of particular interest is the azimuthal anisotropy of particles containing charm and beauty quarks. Because these heavy quarks have masses greater than the initial temperature of the QGP and the  $\Lambda_{QCD}$  scale, they are produced in the initial parton-parton hard scatterings and their production can be described [6] by perturbative QCD. Once produced, the heavy quarks

cannot be destroyed by the QGP and will experience the whole evolution of the system, giving access to QGP transport properties [7].

Previous PHENIX measurements of cross sections of electrons from separated charm and beauty decays suggest a stronger suppression of charmed hadrons than for beauty hadrons [8, 9]. This indicates a mass ordering of the quark interactions with the QGP medium. The specific mechanisms that contribute to how heavy quarks interact with the QGP are still not entirely understood. Different effects such as radiative [10, 11] and collisional [12] energy loss dominate the interactions depending on the heavy-quark transverse momentum. Low- $p_T$  charm and beauty quarks relevant to our measurement are nonrelativistic, and their propagation and interaction with the medium gives access to the drag and diffusion-transport coefficients of the QGP [13]. It is important to understand if and how heavy quarks equilibrate with the QGP, and how hadronization via coalescence [14] of light and heavy quarks may influence the flow of the final-state hadrons. Measurements of collective flow of light and heavy hadrons in different kinematic regions may help answer these questions.

Much work has been done at the Relativistic Heavy Ion Collider (RHIC) to study the azimuthal anisotropy of heavy-flavor particles at midrapidity [8, 15, 16]. These previous RHIC results show a nonzero elliptic flow for heavy-flavor particles and a clear mass ordering between heavy and light hadrons. However, there have been no RHIC measurements of elliptic flow of heavy-flavor particles at forward rapidity. Particles produced at forward rapidity sample a different area of phase space than those produced at midrapidity and could also be subject

\* Deceased

† PHENIX Spokesperson: akiba@rcf.rhic.bnl.gov

to different pressure gradients and temperatures within the QGP. This makes forward-rapidity measurements an important part of understanding particle interactions with the medium. At the LHC, the forward rapidity ( $1 < |\eta| < 2$ ) and midrapidity measurements ( $|\eta| < 1$ ) of open-heavy-flavor  $v_2$  [17] show a similar trend. However, the boost-invariant region of QGP is much wider at the LHC than at RHIC due to the higher center-of-mass energies. Heavy-flavor production rates and the QGP temperature are significantly different between RHIC and the LHC. Therefore, these forward-rapidity measurements at RHIC energies are needed.

The organization of this paper is as follows. Section II describes the PHENIX detector with special detail paid to the forward-rapidity detectors that are crucial for this analysis. Sections III and IV describe the experimental methods and procedure. Section V presents the first measurements at RHIC energies of the  $v_2$  of decay muons from open-heavy-flavor mesons at forward rapidity and the measurement of the  $v_2$  of charged hadrons. Finally, Section VI presents conclusions and commentary on the results.

## II. PHENIX DETECTOR

The PHENIX detector [18] comprises the global detectors, the central-arm spectrometers, and the muon-arm spectrometers. The global detectors (the zero-degree calorimeters and the beam-beam counters (BBCs) [19]) are used to define a minimum-bias trigger as well as to determine the primary vertex and charged-particle multiplicity [19].

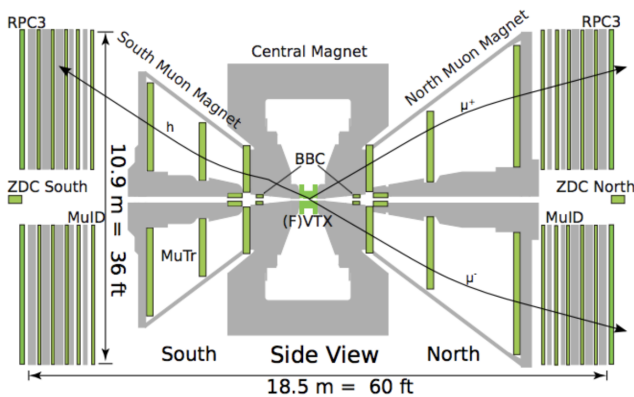


FIG. 1. Side view of the PHENIX detector.

The central-arm spectrometers provide precise tracking and particle identification for electrons, charged hadrons, and photons. Tracking and momentum determination are provided by drift chambers and pad chambers. Particle identification is provided by time of flight, ring-imaging Čerenkov detectors, and electromagnetic calorimeters. The BBCs and the central-arm tracking detectors are used for event-plane (EP) determination

along with the forward-silicon-vertex detectors (FVTX), as described in Section III. The central-arm silicon-vertex detector (VTX) [20] is used to precisely determine the primary vertex point along the beam axis. Figure 1 shows a side view of the PHENIX detector with the muon-arm spectrometers, BBC, (F)VTX, and the central magnet.

### A. The Muon-arm Spectrometers

The PHENIX muon-arm spectrometers cover a pseudorapidity range of  $1.2 < |\eta| < 2.2$  and full  $2\pi$  in azimuth. Each muon spectrometer comprises hadron-absorbing material, muon trackers (MuTr) inside a conical-shaped magnet, and a muon identifier (MuID) [21]. Separate from the spectrometers, but crucial for this analysis, is the forward-silicon-vertex detector (FVTX) [22]. The first layer of hadron-absorber material is placed between the FVTX and MuTr comprising 19 cm of copper, followed by 60 cm of iron from the central magnet, and then 36.2 cm of steel, all of which correspond to 7.2 nuclear-interaction lengths. This absorbing material is meant to block pions and kaons emitted into the acceptance range of the spectrometers, but allow muons to penetrate. Tracking and momentum measurements are performed by the MuTr that comprises eight octants of cathode-strip chambers in three different stations. The momentum resolution achieved by the MuTr is approximately  $\delta p/p = 0.05$  for muons. The MuID system is located downstream of the MuTr and contains five absorber plates in addition to the absorber material before the MuTr. Two Iarocci tube planes with vertical and horizontal orientations are placed after each of the five absorber plates. The general operating principle is that hadrons that manage to penetrate the initial absorbing layers between the FVTX and MuTr will not penetrate all of the MuID absorption plates, whereas muons will penetrate all the plates and leave signals in the final set of Iarocci tubes.

### B. Silicon Vertex Detectors (F)VTX

The silicon-vertex detector (VTX) has four radial layers placed at 2.6, 5.1, 11.8, 16.7 cm from the  $z$ -axis covering  $2 \times \Delta\phi \approx 1.6\pi$  and  $|z_{\text{vtx}}| < 10$  cm. The forward VTX detector (FVTX) [22] is a silicon-strip detector comprising four layers at 20.1, 26.1, 32.2, and 38.2 cm along the  $z$ -axis that measure particle trajectories. The VTX and FVTX measure the radial distance of closest approach ( $DCA_R$ , which is determined by projecting the particle track from the FVTX onto a plane in the  $z$ -axis located at the primary vertex point determined by the VTX. Precisely measuring  $DCA_R$  allows for a statistical separation of muons from short-lived particles, like heavy-flavor mesons, and those from long-lived particles such as pions and kaons. The PYTHIA+GEANT4 simulations show that selecting particles with  $|DCA_R| < 500$

$\mu\text{m}$  (Fig. 3) greatly increases the purity of the measured sample of heavy-flavor muons.

### III. ANALYSIS METHODS

Au+Au collisions at  $\sqrt{s_{NN}} = 200$  GeV are measured using data collected at RHIC during 2014 and 2016 with a combined integrated luminosity of  $14.5 \text{ nb}^{-1}$ . The analysis was performed for charged hadrons and muons over the transverse momentum range  $1 < p_T < 4 \text{ GeV}/c$  with tracks being required to have multiple hits in the FVTX, MuTr, and MuID as described below.

#### A. Event and track selection

The large amount of absorbing material between the FVTX and MuTr is effective at stopping hadrons, but it also causes significant issues with matching tracks between the two detectors. Particles can undergo multiple scatterings in the absorbing material causing a single MuTr track to be matched with multiple FVTX tracks. A ‘‘mixed-event’’ subtraction technique is employed to precisely estimate the substantial background from mismatched tracks and multiple scatterings.

We quantify the quality of MuTr-FVTX track matching with the  $\chi^2$ -FVTXMuTr variable, which includes the residuals between the track projections in three different Z planes between FVTX and MuTr. The  $\chi^2$ -FVTXMuTr distribution of same-event matching include true associations, where the MuTr track and the FVTX track correspond to the same particle, and ‘‘fake’’ matchings, for which the MuTr and FVTX tracks are from different particles. The  $\chi^2$ -FVTXMuTr distribution of mixed-event associations include only fake matchings. Mixed-event associations are constructed from events that have a similar Z-vertex and event centrality. The same-event  $\chi^2$ -FVTXMuTr distribution is described by the function:  $f(\chi^2) = f_{\text{true}}(\chi^2) + f_{\text{fake}}(\chi^2)$ , where  $f_{\text{true}}$  and  $f_{\text{fake}}$  represent the true and fake associations, respectively. The line shape of  $f_{\text{fake}}$  is obtained from mixed-event matchings. A Landau distribution best represents  $f_{\text{true}}$ , regardless the of the  $p_T$  of the muon and the event centrality. The function  $f(\chi^2)$  is fit to the same-event  $\chi^2$ -FVTXMuTr distribution as shown in Fig. 4. The integral of  $f_{\text{true}}$  corresponds to the yield of particles measured by the MuTr and FVTX coming from the vertex.

Loose track-selection criteria are used for signal extraction. Then, the selections detailed in Table I are applied to maximize signal over background in the sample. These selections were determined using full GEANT4 simulations.

The variables for the event- and track-selection criteria that are tabulated in Table I are:

**BBC<sub>z</sub>:** The  $z$  vertex position of the initial collision point as determined by the BBCs

TABLE I. Event- and track-selection criteria.

| Variable           | South arm       | North arm       |
|--------------------|-----------------|-----------------|
| Centrality         | 0%–70%          | 0%–70%          |
| BBC <sub>z</sub>   | <10 cm          | <10 cm          |
| DCA <sub>R</sub>   | <0.05 cm        | <0.05 cm        |
| $\chi^2$ -FVTXMuTr | < 3             | < 3             |
| pDG0               | <60 mm· GeV/c   | <35 mm· GeV/c   |
| pDDG0              | <40 mrad· GeV/c | <40 mrad· GeV/c |
| MuTr $\chi^2$      | < 5             | < 5             |
| MuTrhits           | $\geq 14$       | $\geq 16$       |
| MuIDhits           | $\geq$          | $\geq 4$        |
| MuID $\chi^2$      | < 5             | < 5             |
| pz                 | >3 GeV/c        | >3.6 GeV/c      |
| lastgap            | = 2, 3, or 4    | = 2, 3, or 4    |

**DCA<sub>R</sub>:** Radial distance of closest approach (i.e., the measure of the distance from initial collision point at which the particle is produced)

**$\chi^2$ -FVTXMuTr:** Quality of track matching between FVTX and MuTr

**DG0:** Distance between MuID 1st hit and extrapolated track

**DDG0:** Angular distance between MuID 1st hit and extrapolated track

**MuTr $\chi^2$ :** Quality of matching between reconstructed track projection and hits in the MuTr

**MuTrhits:** Number of MuTr hits for particle

**MuIDhits:** Number of MuID hits for particle

**MuID $\chi^2$ :** Quality of matching between reconstructed track projection and hits in the MuID

**pz:** Particle  $z$  momentum

**lastgap:** Last hit position in MuID

#### B. Event-plane method and azimuthal-anisotropy measurements

In an off-center collision of two nuclei the reaction plane is defined as the plane formed by the impact parameter vector and the initial collision axis for each event. In practice, the reaction plane is not directly observable, but the azimuthal distribution of the particles detected in the final state can be used to determine the EP that contains both the beam direction and the azimuthal direction of maximum particle density. The event-flow vector  $Q_n$  and the EP angle  $\Psi_n$  for each  $n^{\text{th}}$  harmonic are defined by the following:

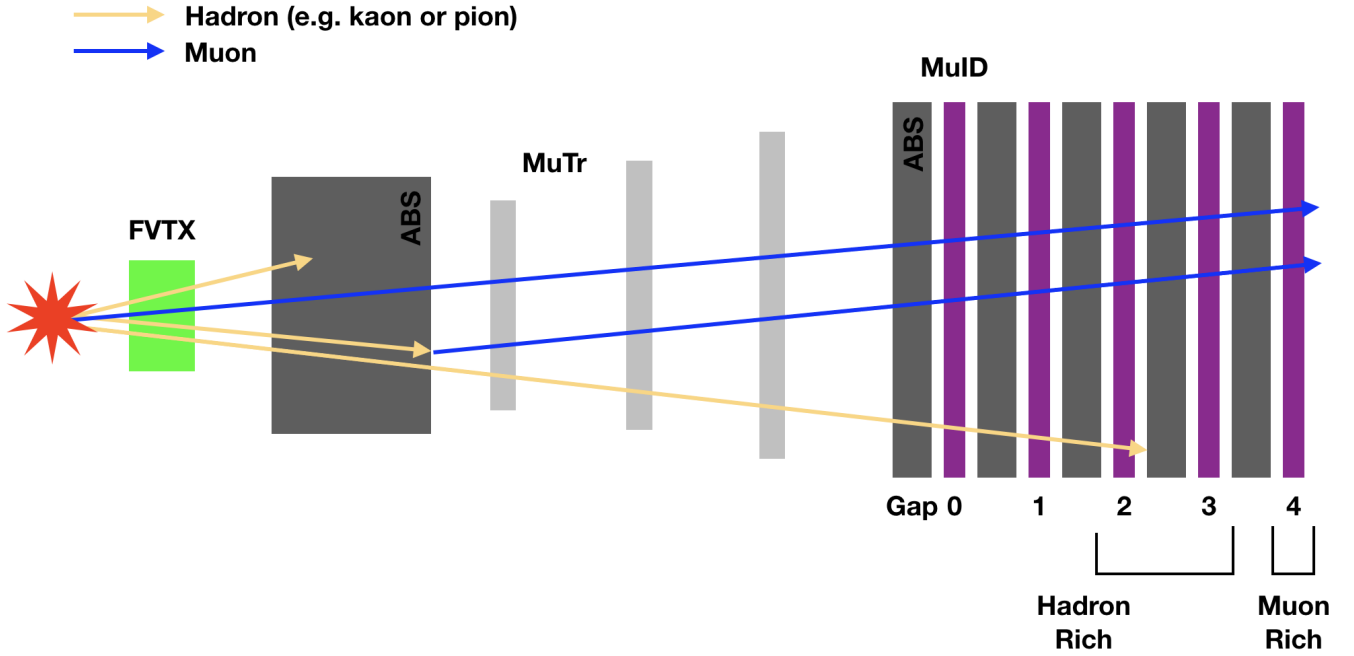


FIG. 2. Schematic of hadron and muon propagation through the PHENIX FVTX and muon spectrometers. Muons will penetrate all absorber layers leaving hits in the FVTX, MuTr, and final layer of the MuID, whereas hadrons will be stopped by one of the absorber layers.

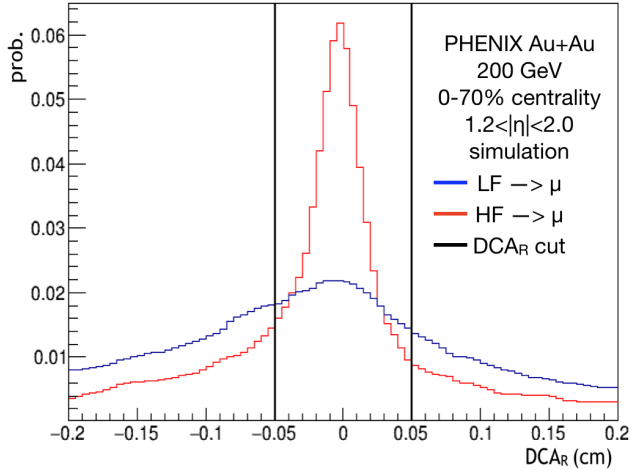


FIG. 3. PYTHIA+GEANT4 simulation of decay muons from light (LF) and heavy-flavor (HF) hadrons. Both distributions are normalized to one and we see that at  $DCA_R$  values close to zero ( $|DCA_R| < 0.05$  cm) muons from heavy-flavor hadrons are enriched relative to those from light hadrons.

$$Q_x = \sum_i \cos(n\phi_i) \quad Q_y = \sum_i \sin(n\phi_i) \quad (2)$$

$$\Psi_n = \text{atan}(Q_y/Q_x), \quad (3)$$

where  $\phi_i$  are the azimuthal angles of the particles used for EP determination.

The  $v_n$  observed with respect to the event plane is given by:

$$v_n^{\text{obs}} = \langle \cos[n(\phi - \Psi_n)] \rangle, \quad (4)$$

where  $\langle \rangle$  denotes an average over all particles and all selected collision events. The true flow is obtained by

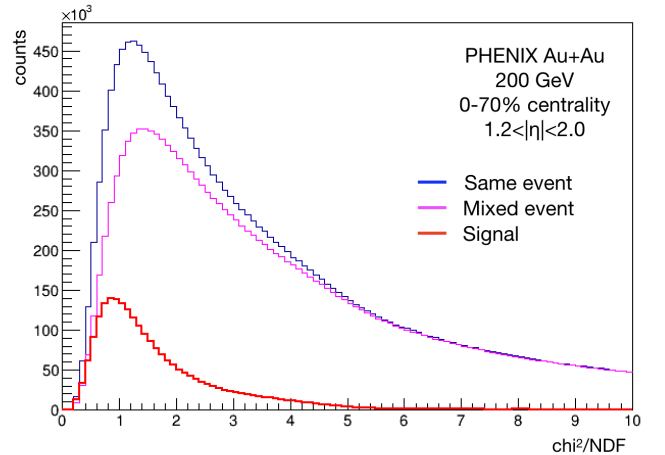


FIG. 4. The  $\chi^2$ -FVTXMuTr distributions for the same- and mixed-event matchings with the signal extracted from the fit.

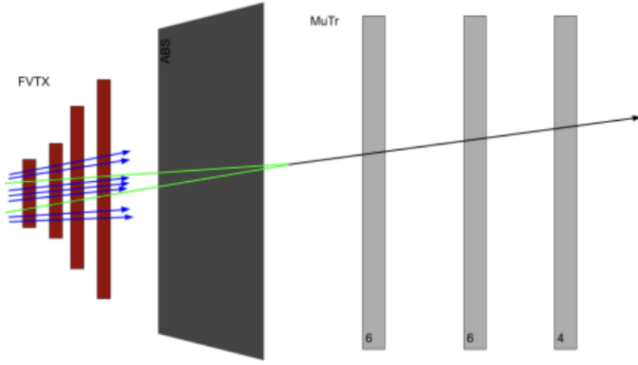


FIG. 5. Illustration of a single MuTr track being matched with all FVTX tracks within  $2\sigma$  of the residual  $\eta$  and  $\phi$  distribution determined by the FVTX and MuTr.

dividing the observed flow by the corresponding EP resolution.

$$v_n = \frac{v_n^{\text{obs}}}{\mathcal{R}_n} \quad (5)$$

The second-order EP angle,  $\Psi_2$ , is measured using the FVTX detectors on the north and south sides of the central-arm spectrometers. To avoid short-range correlations that are not associated with the collective flow, it is critical to have a large rapidity gap between the detector used to determine the event plane and the detector used in the flow measurement. Thus, particles detected in the north muon arm are correlated with the event plane measured in the south FVTX, and vice versa. The event-plane resolution is estimated using the three subevent method [23].

$$\mathcal{R}_2^a = \sqrt{\frac{\langle \cos(2(\Psi_a - \Psi_b)) \rangle \langle \cos(2(\Psi_a - \Psi_c)) \rangle}{\langle \cos(2(\Psi_b - \Psi_c)) \rangle}} \quad (6)$$

Following the determination of the EP angle and associated resolution, the azimuthal anisotropy is measured by counting the number of particles in different  $\Delta\phi$  bins relative to the event-plane angle. By distinguishing the azimuthal angle of emission for each individual particle as either “in-plane” or “out-of-plane” relative to the event plane angle (Fig. 6) the azimuthal anisotropy is determined for a given transverse-momentum bin by:

$$v_2^{\text{obs}} = \frac{\pi}{4} \frac{N_{\text{in}} - N_{\text{out}}}{N_{\text{in}} + N_{\text{out}}} \quad (7)$$

The statistical uncertainties  $\sigma_{\text{in}}$  and  $\sigma_{\text{out}}$  in the number of particles detected in-plane and out-of-plane ( $N_{\text{in}}$  and  $N_{\text{out}}$ ) are propagated to the uncertainty  $\sigma_{v_2^{\text{obs}}}$  in the  $v_2^{\text{obs}}$  measurement.

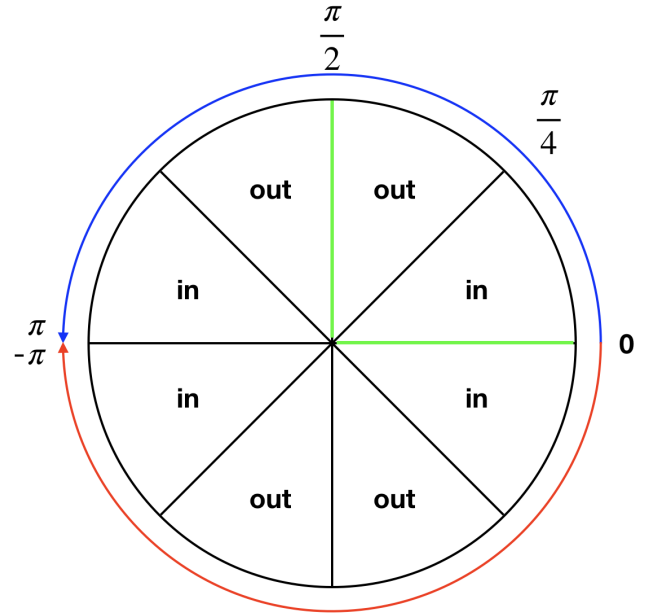


FIG. 6. Diagram of in plane and out of plane particle emission relative to the EP angle.

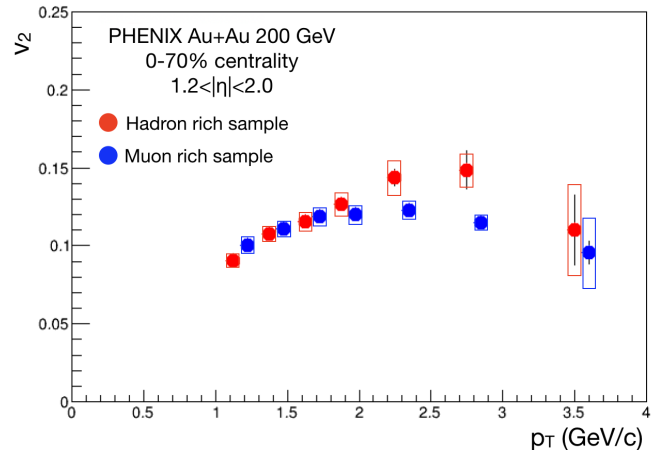


FIG. 7. Elliptic flow of charged particles in hadron-rich and muon-rich samples. For clarity the data for the muon-rich sample are offset by 0.1 GeV/c to higher  $p_T$ .

$$\sigma_{v_2^{\text{obs}}} = \frac{\pi}{2(N_{\text{in}} + N_{\text{out}})^2} \cdot \sqrt{(N_{\text{out}}\sigma_{\text{in}})^2 + (N_{\text{in}}\sigma_{\text{out}})^2} \quad (8)$$

#### IV. ANALYSIS PROCEDURE

We separate the particles into two distinct samples: (i) the light-hadron-rich sample comprises particles that stop in the second and third layers of the MuID; and (ii) the muon-rich sample comprising particles which can penetrate the third or fourth layer of the MuID. Using

the method described in Section III we measure  $v_2$  of both samples as shown in Fig. 7.

A full PYTHIA3+GEANT4 [24, 25] detector simulation was employed to determine the particle composition of both samples. Detectable particles are generated by PYTHIA3, they include kaons, pions, protons, and muons. The  $K/\pi$ ,  $K^+/K^-$ , and  $\pi^+/\pi^-$  yield ratios provided by PYTHIA3 are modified according to extrapolations based on measurements performed at midrapidity by PHENIX [26], and at forward rapidity by BRAHMS [27] in Au+Au collisions at  $\sqrt{s_{NN}}=200$  GeV. The charged particle  $p_T$  distribution is also weighted according to PHENIX and BRAHMS data. PYTHIA3 events containing these detectable particles are used as input to the GEANT4-based detector simulation. Approximately  $10^{-4}$  of the light hadrons can penetrate the first muon-spectrometer absorber. Only events where at least one of the particles produces more than two hits in the MuTr detector volume are kept. Fewer than 2% of the hadrons producing hits in MuTr are estimated to be protons, thus they were excluded in this analysis. The GEANT hits are then merged with hits from a minimum-bias real-data event and reconstructed by the tracking algorithms. Figure 8 shows the composition of light hadrons and muons in samples (i) and (ii) as a function of reconstructed track  $p_T$  as obtained from the full PYTHIA3+GEANT4 simulation.

The  $v_2$  of hadron-rich ( $v_2^{h\text{-rich}}$ ) and muon-rich ( $v_2^{\mu\text{-rich}}$ ) samples are composed by the following terms:

$$v_2^{h\text{-rich}} = \frac{N_h^{h\text{-rich}}}{N^{h\text{-rich}}} v_2^h + \frac{N_\mu^{h\text{-rich}}}{N^{h\text{-rich}}} v_2^\mu \quad (9)$$

$$v_2^{\mu\text{-rich}} = \frac{N_h^{\mu\text{-rich}}}{N^{\mu\text{-rich}}} v_2^h + \frac{N_\mu^{\mu\text{-rich}}}{N^{\mu\text{-rich}}} v_2^\mu, \quad (10)$$

where the fractions are the light-hadron and muon compositions of both samples as shown in Fig. 8. The light-hadron and muon-elliptic-flow values  $v_2^h$  and  $v_2^\mu$  are obtained by solving the set of equations 9 and 10.

The muon sample comprises light-hadron decays and heavy-flavor decays. Therefore, its flow can be determined as:

$$v_2^\mu = F_{\text{HF}} v_2^{\text{HF}} + (1 - F_{\text{HF}}) v_2^{h \rightarrow \mu} \quad (11)$$

$$F_{\text{HF}} = \frac{N_{\text{HF} \rightarrow \mu}}{N_{\text{LH} \rightarrow \mu} + N_{\text{HF} \rightarrow \mu}}, \quad (12)$$

where  $F_{\text{HF}}$  is the heavy-flavor-decay contribution to the muon sample, and  $v_2^{h \rightarrow \mu}$  is the elliptic flow of muons from light-hadron decays. The light-hadron contribution  $N_{\text{LH} \rightarrow \mu}$  to the muon-rich sample is obtained from the detector simulation using as input the measured counts in the light-hadron sample  $N^{h\text{-rich}}$ . The light-hadron extrapolation and fraction  $F_{\text{HF}}$  are shown in Fig. 9. The elliptic flow  $v_2^{h \rightarrow \mu}$  of muons from light-hadron decays seen

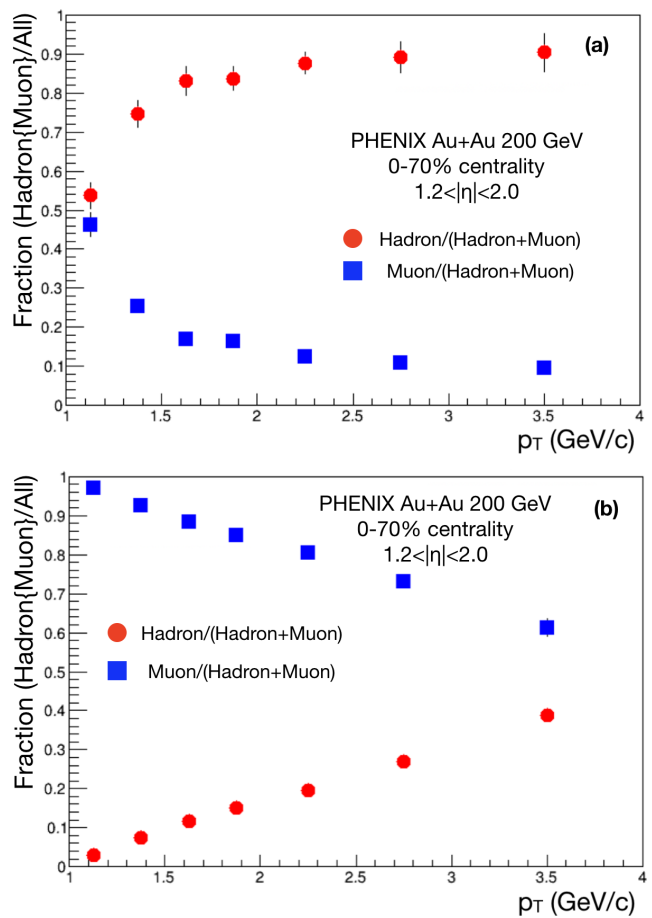


FIG. 8. Hadron and muon particle fractions as a function of  $p_T$  for (a) particles that stop in the second and third layer of the MuID (hadron-rich sample), and (b) particles that penetrate the third and fourth layer of the MuID (muon-rich sample).

in the muon-rich sample is also determined from the detector simulation, where the generated hadron sample input is modulated as  $dN/d\Delta\phi = v_2^h \cos(2\Delta\phi)$ .

## A. Simulation studies

### B. Systematic uncertainties for $v_2$

Four main sources of systematic uncertainties were considered: background determination, track selections, particle composition, and event-plane determination.

#### 1. Background determination

We evaluate the uncertainty that the background-normalization method introduces to the measurement of  $v_2$ . In Section III the signal is obtained after determining a  $p_T$ -dependent normalization scale for the mixed-



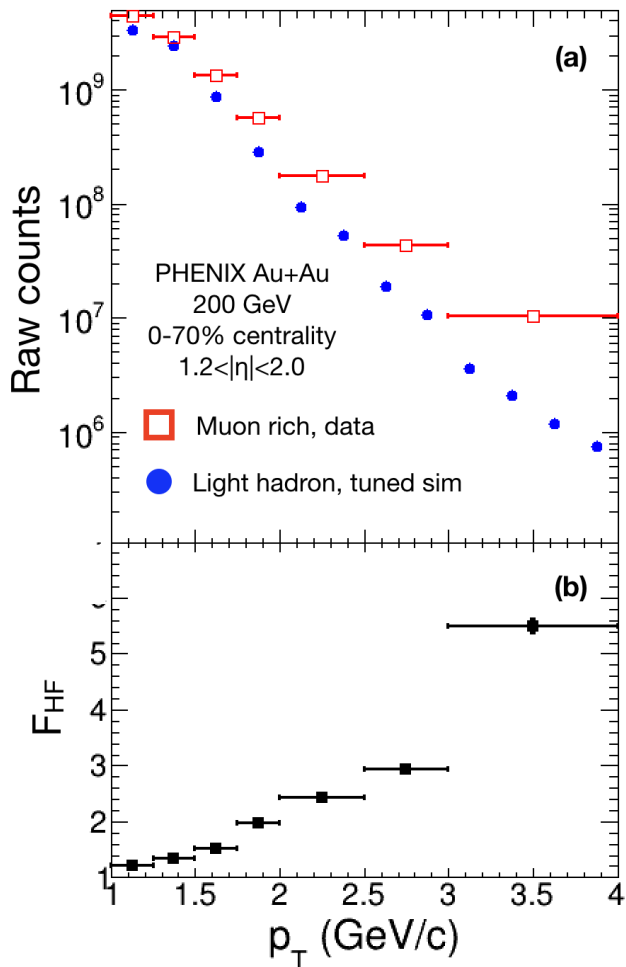


FIG. 9. The muon-rich data compared to muon-rich simulation (with heavy-flavor contribution excluded) and the associated heavy-flavor fraction as a function of  $p_T$ .

event sample. This method assumes that the range where the  $\chi^2$ -FVTXMuTr distribution is fitted to obtain the normalization is dominated by background both in the same-event and in the mixed-event samples. To account for the uncertainties associated with this assumption, the normalization factor was increased and decreased by two standard deviations of the value returned by the fit. Then, the remainder of the analysis was performed identically. Any difference in the final  $v_2$  value is due to the background-normalization factor.

## 2. Track selections

There are numerous track selections that are used to improve the signal over background in the dataset and to exclude misreconstructed particles. To determine the influence of these selections on the final  $v_2$  values, the analysis was repeatedly performed by independently varying each cut. Because these cuts are all correlated, the largest

difference for each  $p_T$  bin was taken as the associated systematic uncertainty.

## 3. Particle composition

Another source of systematic uncertainty is associated with the particle composition in the simulations described in Sec. IV. The particle composition was tuned to match previously published PHENIX [26] results from Au+Au collisions for kaon and pion ratios, as well as charged hadron spectra. However, these results are from midrapidity ( $|\eta| < 0.35$ ) measurements, unlike our analysis. The  $p_T$ -integrated forward-rapidity measurements from BRAHMS [27] indicated no strong rapidity dependence for kaon and pion ratios. As a systematic check, we varied the particle ratios in the simulation within the uncertainties of the BRAHMS results and remeasured the  $v_2$ . Additional uncertainties arise from using the tuned simulation to decompose the  $v_2$  measurements into hadron and muon contributions and counting the number of hadrons and muons in any given  $p_T$  bin. These two uncertainties are added in quadrature to obtain the total systematic uncertainty from particle composition.

## 4. Event-plane determination

In the standard analysis we use the FVTX to determine the EP angle and the muon arm opposite to the event-plane detector to measure  $v_2$ . To evaluate how various detector inefficiencies and differences in rapidity gaps between the muon detectors and the detectors used to determine the EP angle influence the final  $v_2$  results, a different set of detectors was used to perform the measurement. Namely, the analysis was performed again using the central-arm tracking detectors ( $|\eta| < 0.35$ ) as the event-plane detector for both north and south muon-arm measurements.

## 5. Total systematic uncertainty

The relative systematic uncertainty from each source is listed in Table II. Independent evaluations for each of the sources were added in quadrature to obtain the total systematic uncertainty of the  $v_2$  measurements.

## V. RESULTS AND DISCUSSION

The  $v_2$  measurements in the PHENIX muon arms for charged hadrons and open-heavy-flavor muons are presented here as a function of  $p_T$  ( $1.2 < |\eta| < 2.0$ ). The results are compared to previous PHENIX measurements [28] at midrapidity ( $|\eta| < 0.35$ ). Figure 10 shows the measurements of  $v_2(p_T)$  for charged hadrons.

TABLE II. Relative systematic uncertainty in percent for the measurements of  $v_2$  for hadrons and heavy-flavor muons.

| $p_T$ [GeV/c] | Background | Composition | Track cuts | EP  |
|---------------|------------|-------------|------------|-----|
| 1.00–1.25     | 1.0        | 4.4         | 4.7        | 1.0 |
| 1.25–1.50     | 0.9        | 4.5         | 3.5        | 0.5 |
| 1.50–1.75     | 0.6        | 4.6         | 4.3        | 0.9 |
| 1.75–2.00     | 0.6        | 4.3         | 6.0        | 4.3 |
| 2.00–2.50     | 0.2        | 4.1         | 4.0        | 1.3 |
| 2.50–3.00     | 0.4        | 5.6         | 4.3        | 14  |
| 3.00–4.00     | 13         | 6.3         | 20         | 8.0 |

The values of  $v_2(p_T)$  at forward rapidity are systematically below those at midrapidity by about 10%. This is comparable to the size of systematic uncertainties, which are point-to-point correlated. The PHOBOS results on the rapidity dependence of  $p_T$ -integrated-charged-hadron  $v_2$  [29] show a similar decrease in  $v_2$  between the rapidity ranges of the PHENIX measurements. A caveat to the  $v_2(p_T)$  comparison is that our forward rapidity measurement does not include protons and antiprotons that are included in the charged-hadron measurements at midrapidity. In the higher-transverse-momentum range ( $p_T > 2$  GeV/c) at midrapidity there will be a proton contribution to the charged-hadron  $v_2$  as the proton/pion ratio increases in this range [30].

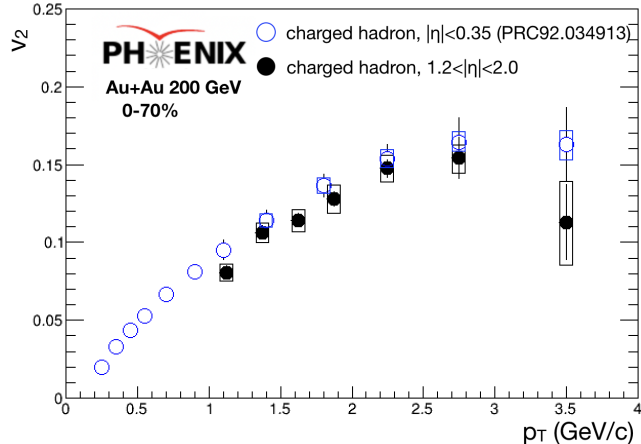


FIG. 10. The value of  $v_2(p_T)$  of charged hadrons at forward rapidity compared to previous midrapidity results. The error bars show statistical uncertainty and the boxes show systematic uncertainties

Figure 11 shows the  $v_2$  of open-heavy-flavor muons at forward rapidity compared to charged hadrons in the same rapidity range and previous PHENIX results of open-heavy-flavor electrons at midrapidity [15]. The heavy-flavor muons exhibit smaller  $v_2$  than the light hadrons, which is to be expected given the mass ordering of particle interactions with the QGP. Similar to the observations in the charged-hadron measurement, there

is no pronounced rapidity dependence for open-heavy-flavor flow. There appears to be a slight shift to higher  $p_T$  in the results for heavy-flavor muons as compared to heavy-flavor electrons. This may be due to the large mass difference between the decay leptons. Despite this apparent shift, the heavy-flavor electron and muon  $v_2(p_T)$  have similar magnitude indicating no clear difference in heavy-quark interactions with the QGP in the measured rapidity range.

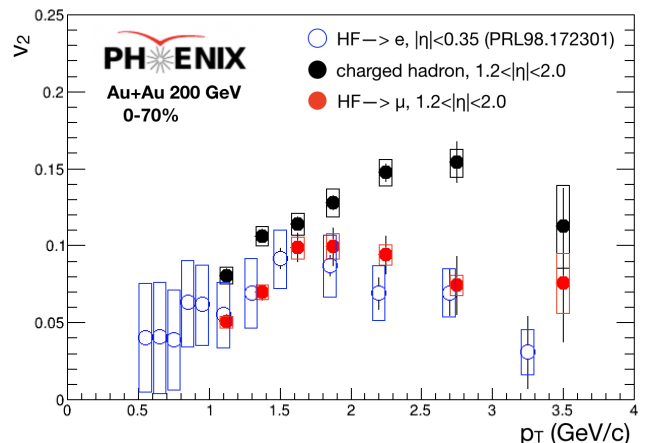


FIG. 11. The value of  $v_2(p_T)$  of heavy-flavor muons and charged hadrons at forward rapidity and heavy-flavor electrons at midrapidity.

## VI. SUMMARY

We have measured the elliptic anisotropy,  $v_2$ , of charged hadrons and open-heavy-flavor muons in Au+Au collisions at  $\sqrt{s_{NN}} = 200$  GeV at forward rapidity ( $1.2 < |\eta| < 2.0$ ). The measurements were performed using data sets collected in 2014 and 2016 corresponding to an integrated luminosity of  $14.5 \text{ nb}^{-1}$ . This is the largest Au+Au data set collected by PHENIX. Measuring  $DCA_R$  with the PHENIX (F)VTX detectors and a mixed-event method successfully overcame the large background in the heavy-flavor-muon sample originating from light-hadron decays and track mismatching before and after the hadron absorber. Using samples detected in different regions of the muon-identification detectors, the light hadrons were separated from inclusive muons, and the heavy-flavor-muon contributions were extracted.

The values of  $v_2(p_T)$  of charged hadrons at forward rapidity appear to be systematically lower than previously published PHENIX results at midrapidity [28] and consistent with expectations from the PHOBOS measurement [29] of the rapidity dependence of charged hadrons. A significant elliptic flow  $v_2(p_T)$  was seen in the open-heavy-flavor-muon sample. A clear difference was observed between the flow of charged hadrons and the muons from heavy-flavor-hadron decays. This differ-

ence suggests that there is a quark-mass dependence of the particle interactions with the QGP. The open-heavy-flavor muon  $v_2$  is comparable in magnitude to previous PHENIX measurements of  $v_2$  of open-heavy-flavor electrons at midrapidity [15]. Taken together, the charged-hadron and the heavy-flavor-muon measurements suggest that there is no strong rapidity dependence in the collective flow of light- and heavy-flavor hadrons in the measured rapidity range at RHIC energies.

## ACKNOWLEDGMENTS

We thank the staff of the Collider-Accelerator and Physics Departments at Brookhaven National Laboratory and the staff of the other PHENIX participating institutions for their vital contributions. We acknowledge support from the Office of Nuclear Physics in the Office of Science of the Department of Energy, the National Science Foundation, Abilene Christian University Research Council, Research Foundation of SUNY, and Dean of the College of Arts and Sciences, Vanderbilt University (USA), Ministry of Education, Culture, Sports,

Science, and Technology and the Japan Society for the Promotion of Science (Japan), Natural Science Foundation of China (People's Republic of China), Croatian Science Foundation and Ministry of Science and Education (Croatia), Ministry of Education, Youth and Sports (Czech Republic), Centre National de la Recherche Scientifique, Commissariat à l'Énergie Atomique, and Institut National de Physique Nucléaire et de Physique des Particules (France), J. Bolyai Research Scholarship, EFOP, HUN-REN ATOMKI, NKFIH, and OTKA (Hungary), Department of Atomic Energy and Department of Science and Technology (India), Israel Science Foundation (Israel), Basic Science Research and SRC(CENuM) Programs through NRF funded by the Ministry of Education and the Ministry of Science and ICT (Korea), Ministry of Education and Science, Russian Academy of Sciences, Federal Agency of Atomic Energy (Russia), VR and Wallenberg Foundation (Sweden), University of Zambia, the Government of the Republic of Zambia (Zambia), the U.S. Civilian Research and Development Foundation for the Independent States of the Former Soviet Union, the Hungarian American Enterprise Scholarship Fund, the US-Hungarian Fulbright Foundation, and the US-Israel Binational Science Foundation.

- 
- [1] K. Adcox *et al.* (PHENIX Collaboration), Formation of dense partonic matter in relativistic nucleus-nucleus collisions at RHIC: Experimental evaluation by the PHENIX collaboration, *Nucl. Phys. A* **757**, 184 (2005).
- [2] I. Arsene *et al.* (BRAHMS Collaboration), Quark gluon plasma and color glass condensate at RHIC? The Perspective from the BRAHMS experiment, *Nucl. Phys. A* **757**, 1 (2005).
- [3] B. B. Back *et al.* (PHOBOS Collaboration), The PHOBOS perspective on discoveries at RHIC, *Nucl. Phys. A* **757**, 28 (2005).
- [4] J. Adams *et al.* (STAR Collaboration), Experimental and theoretical challenges in the search for the quark gluon plasma: The STAR Collaboration's critical assessment of the evidence from RHIC collisions, *Nucl. Phys. A* **757**, 102 (2005).
- [5] E. V. Shuryak, What RHIC experiments and theory tell us about properties of quark-gluon plasma?, *Nucl. Phys. A* **750**, 64 (2005).
- [6] M. Cacciari, P. Nason, and R. Vogt, QCD predictions for charm and bottom production at RHIC, *Phys. Rev. Lett.* **95**, 122001 (2005).
- [7] X. Dong, Y.-J. Lee, and R. Rapp, Open heavy-flavor production in heavy-ion collisions, *Annual Review of Nuclear and Particle Science* **69**, 417 (2019).
- [8] A. Adare *et al.* (PHENIX Collaboration), Single electron yields from semileptonic charm and bottom hadron decays in Au+Au collisions at  $\sqrt{s_{NN}} = 200$  GeV, *Phys. Rev. C* **93**, 034904 (2016).
- [9] N. J. Abdulmeher *et al.* (PHENIX Collaboration), Charm- and bottom-quark production in Au+Au collisions at  $\sqrt{s_{NN}} = 200$  GeV, *Phys. Rev. C* **109**, 044907 (2024).
- [10] M. G. Mustafa, D. Pal, D. K. Srivastava, and M. Thoma, Radiative energy loss of heavy quarks in a quark gluon plasma, *Phys. Lett. B* **428**, 234 (1998).
- [11] Y. L. Dokshitzer and D. E. Kharzeev, Heavy quark colorimetry of QCD matter, *Phys. Lett. B* **519**, 199 (2001).
- [12] A. Meistrenko, A. Peshier, J. Uphoff, and C. Greiner, Collisional energy loss of heavy quarks, *Nucl. Phys. A* **901**, 51 (2013).
- [13] S. Cao *et al.*, Toward the determination of heavy-quark transport coefficients in quark-gluon plasma, *Phys. Rev. C* **99**, 054907 (2019).
- [14] M. He and R. Rapp, Hadronization and Charm-Hadron Ratios in Heavy-Ion Collisions, *Phys. Rev. Lett.* **124**, 042301 (2020).
- [15] A. Adare *et al.* (PHENIX Collaboration), Energy Loss and Flow of Heavy Quarks in Au+Au Collisions at  $\sqrt{s_{NN}} = 200$  GeV, *Phys. Rev. Lett.* **98**, 172301 (2007).
- [16] L. Adamczyk *et al.* (STAR Collaboration), Measurement of  $D^0$  Azimuthal Anisotropy at Midrapidity in Au+Au Collisions at  $\sqrt{s_{NN}}=200$  GeV, *Nucl. Instrum. Methods Phys. Res., Sec. A* **118**, 212301 (2017).
- [17] A. M. Sirunyan *et al.* (CMS Collaboration), Measurement of prompt  $D^0$  and  $\bar{D}^0$  meson azimuthal anisotropy and search for strong electric fields in PbPb collisions at  $\sqrt{s_{NN}} = 5.02$  TeV, *Phys. Lett. B* **816**, 136253 (2021).
- [18] D. P. Morrison *et al.* (PHENIX Collaboration), The PHENIX experiment at RHIC, *Nucl. Phys. A* **638**, 565 (1998).
- [19] M. Allen *et al.* (PHENIX Collaboration), Phenix inner detectors, *Nucl. Instrum. Methods Phys. Res., Sec. A* **499**, 549 (2003).
- [20] R. Nouicer (PHENIX Collaboration), PHENIX Upgrade: Novel Stripixel Detector for Heavy Quark Detection and

- Proton Spin Structure Measurements at RHIC Energies, Nucl. Instrum. Methods Phys. Res., Sec. B **261**, 1067 (2007).
- [21] H. Akikawa *et al.* (PHENIX Collaboration), PHENIX muon arms, Nucl. Instrum. Methods Phys. Res., Sec. A **499**, 537 (2003).
- [22] C. Aidala *et al.* (PHENIX Collaboration), The phenix forward silicon vertex detector, Nucl. Instrum. Methods Phys. Res., Sec. A **755**, 44 (2014).
- [23] A. M. Poskanzer and S. A. Voloshin, Methods for analyzing anisotropic flow in relativistic nuclear collisions, Phys. Rev. C **58**, 1671 (1998).
- [24] C. Bierlich *et al.*, A comprehensive guide to the physics and usage of PYTHIA 8.3, SciPost Phys. Codebases **2022**, 8 (2022).
- [25] S. Agostinelli *et al.* (GEANT4 Collaboration), GEANT4—a simulation toolkit, Nucl. Instrum. Methods Phys. Res., Sec. A **506**, 250 (2003).
- [26] A. Adare *et al.* (PHENIX Collaboration), Spectra and ratios of identified particles in Au+Au and d+Au collisions at  $\sqrt{s_{NN}} = 200$  GeV, Phys. Rev. C **88**, 024906 (2013).
- [27] I. C. Arsene *et al.* (BRAHMS Collaboration), Rapidity and centrality dependence of particle production for identified hadrons in Cu+Cu collisions at  $\sqrt{s_{NN}} = 200$  GeV, Phys. Rev. C **94**, 014907 (2016).
- [28] A. Adare *et al.* (PHENIX Collaboration), Systematic Study of Azimuthal Anisotropy in Cu+Cu and Au+Au Collisions at  $\sqrt{s_{NN}} = 62.4$  and 200 GeV, Phys. Rev. C **92**, 034913 (2015).
- [29] B. B. Back *et al.* (PHOBOS Collaboration), Centrality and pseudorapidity dependence of elliptic flow for charged hadrons in Au+Au collisions at  $\sqrt{s_{NN}} = 200$  GeV, Phys. Rev. C **72**, 051901 (2005).
- [30] S. S. Adler *et al.* (PHENIX Collaboration), Identified charged particle spectra and yields in Au+Au collisions at  $\sqrt{s} = 200$  GeV, Phys. Rev. C **69**, 034909 (2004).